High-Speed Melt Spinning of Bicomponent Fibers: Mechanism of Fiber Structure Development in Poly(ethylene terephthalate)/Polypropylene System

TAKESHI KIKUTANI,[1,*] J. RADHAKRISHNAN,[1] SADAAKI ARIKAWA,[1] AKIRA TAKAKU,[1] NORIMASA OKUI,[1] XIA JIN,[2] FUMIO NIWA,[2] and YOSUKE KUDO[2]

[1]Department of Organic and Polymeric Materials, Tokyo Institute of Technology, 2-12-1, O-okayama, Meguro-ku, Tokyo 152, Japan; [2]Specialty Products Development Laboratory, New Oji Paper Co., Ltd., 1-10-6, Shinonome, Koto-ku, Tokyo 135, Japan

SYNOPSIS

High-speed bicomponent spinning of poly(ethylene terephthalate) (PET) (core) and polypropylene (PP) (sheath) was carried out and the structure development in the individual components, PET and PP, was investigated. The orientation and crystallinity development in the PET component was enhanced as compared to that of the single-component spinning while the PP component remained in a low orientation state and had a pseudo-hexagonal crystal structure even at high take-up speeds. To clarify the mutual interaction between the two components in bicomponent spinning, a semiquantitative numerical simulation was performed. The simulation results obtained using the Newtonian fluid model showed that the solidification stress in the PET component was enhanced while that of the PP component was decreased in comparison with the corresponding single-component spinning. This is due to the difference in the temperature dependence of their elongational viscosity. Simulation with an upper-convected Maxwell model as the constitutive equation suggested that significant stress relaxation of the PP component can occur in the spinline if the PET component solidifies earlier than does PP. Based on the structural characterization results and the simulation results, it was concluded that the difference in the activation energy of the elongational viscosity and solidification temperature between the two polymers are the main factors influencing the mutual interaction in the bicomponent spinning process.

INTRODUCTION

The bicomponent melt-spinning process, in which two polymers are coextruded to form a single filament with designed cross-sectional arrangement, has received considerable commercial interest owing to its potential applications in the production of various speciality fibers like crimped fibers, fibers for thermal bonding, electrical conducting fibers, ultra-fine fibers, and fibers with noncircular cross sections, etc.[1] While there exists a large body of information on the various aspects of single-component spinning,[2,3] there is a dearth of published information on the bicomponent spinning process. Moreover, most of the earlier studies on bicomponent extrusion reported in the literature are concerned with the analysis of interface between the two continuous phases[4–10] and the stability of the spinline.[11,12]

It is well known that a significant fiber structure development occurs during the high-speed spinning and that the structure and properties of the as-spun fibers strongly depend on the thermal and stress histories the molten polymer experiences in the spinline.[2] When two polymers are co-extruded as in the case of bicomponent spinning, the stress and thermal histories of each component are expected to be significantly different from those in the single-component spinning because of the mutual interaction of the two components. This may also lead

* To whom correspondence should be addressed.

Journal of Applied Polymer Science, Vol. 62, 1913–1924 (1996)
 CCC 0021-8995/96/111913-12

to a significant difference in the fiber structure development. Thus, by selecting a suitable combination of polymers, it might be possible to improve the structure of high-speed spun fibers. A clear understanding of the underlying mechanism of structure formation vis-à-vis the processing conditions, however, is necessary for the effective control of the fiber structure development and thereby the properties of the as-spun fibers.

Mathematical modeling and process simulation have been found to be useful in evolving the mechanism of fiber structure development in the single-component spinning process.[13,14] Although there are a few published works on the mathematical modeling of bicomponent spinning,[15,16] there have not been any attempts so far to understand the mechanism of fiber structure development in the high-speed melt spinning of sheath–core-type bicomponent fibers.

In the present study, sheath–core type bicomponent fibers of poly(ethylene terephthalate) (PET) and polypropylene (PP) were produced by co-extruding these polymers through an annular die using two different extruders. The structure of the as-spun fibers thus produced at various spinning velocities using an air-jet ejector was investigated in detail. A semiquantitative numerical simulation of the bicomponent spinning process was also performed and a mechanism of fiber structure development was discussed on the basis of the structural characterization data and the simulation results.

EXPERIMENTAL

Bicomponent Spinning

Sheath–core-type bicomponent fibers of PET ([η] = 0.65 dL/g) and PP (MFR = 40) were produced by extruding the melt of PET as the core and PP as the sheath component through an annular-type spinneret using two different extrusion systems (Musashino Kikai Co.) at a temperature of 290°C. Each extrusion system consisted of an extruder and a gear pump. The confluence of the polymers was made in the spinning head, and the coaxially combined polymers were extruded through 24 spinning nozzles of 0.3 mm diameter. Total mass flow rate from each hole was set at 1.0 g/min and PET/PP compositions of 10 : 0, 7 : 3, 5 : 5, 4 : 6, and 0 : 10 were selected. The extruded fibers were drawn-down using an air-ejector placed at 1.5 m below the spinneret. The spinning velocity was varied by changing the air pressure applied to the air-ejector. A schematic illustration of the spinning setup is shown in Figure 1.

Characterization of the As-spun Fibers

Linear Density

Linear density of the as-spun fibers was measured by weighing a 10 m fiber bundle consisting of 24 filaments. Spinning velocity (v) was estimated from the linear density (q) and total mass flow rate (W) based on the equation of continuity, $v = W/q$.

Birefringence

Birefringence of the sheath and core in the bicomponent fiber was measured using an interference microscope (Carl Zeiss Jena) equipped with a polarizing filter based on a method described elsewhere.[17] A typical interference fringe pattern of the bicomponent fiber observed under the microscope is shown in Figure 2. The refractive indices of the sheath and core parts, n_{out} and n_{in}, were obtained using the equations given below:

$$\frac{a_{out}}{A}\frac{\lambda}{2} = (n_{out} - N)(R_{out}^2 - R_{in}^2)^{1/2} \quad (1)$$

$$\frac{a_{in}}{A}\frac{\lambda}{2} = (n_{out} - N)(R_{out} - R_{in}) + (n_{in} - N)R_{in} \quad (2)$$

where a_{out} and a_{in} are the shifts of fringe measured at the interface between the sheath and core and at the center of the fiber, respectively. R_{out} and R_{in} are the inner and outer radii; N, the refractive index of the immersion liquid; and λ, the wavelength of the incident light. Equation (2) allows the estimation of the refractive index of the core component alone by subtracting the retardation effect of the sheath component. The birefringence of the sheath and the core was obtained as the difference between the corresponding refractive indices in the parallel and perpendicular directions to the fiber axis.

Wide-angle X-ray Analysis

Wide-angle X-ray diffraction (WAXD) patterns of as-spun fibers were obtained using a nickel-filtered CuKα X-ray radiation source (Rigaku Denki).

RESULTS AND DISCUSSION

Spinning Velocity

The relation between air pressure applied to the air-ejector and spinning velocity achieved for PET/PP bicomponent spinning is compared with that for the single-component spinning of PET and PP in Figure

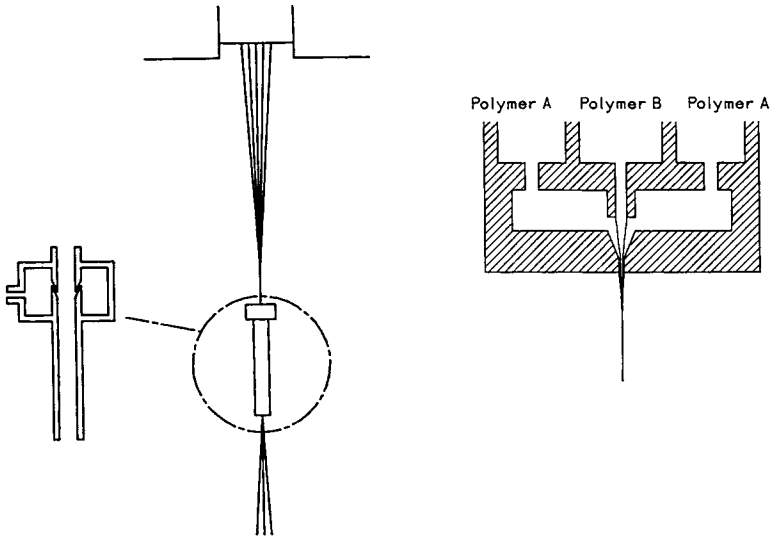

Figure 1 Schematic illustration of the spinning setup.

3. With increase in the air pressure, spinning velocity increased for all the mass flow rate combinations. However, the attained spinning velocities for the PET/PP were lower than those for the corresponding single-component spinning.

Typical photographs of the as-spun single-component and bicomponent fibers are compared in Figure 4. It is worth noting that all the 24 filaments spun simultaneously in the PET/PP bicomponent spinning bonded together and formed a bundle as it emerged out of the air-ejector, whereas the PP and PET single-component fibers were separated from each other. The relatively low spinning velocity attained by the PET/PP bicomponent fibers, in comparison with the single-component fibers, is apparently due to the bundle formation as it leads to the reduction of the total surface area of the filaments and eventually to the reduction of the air-drag force applied by the air-ejector.

Considering the spinning conditions used in this work, the temperature of the running filament at

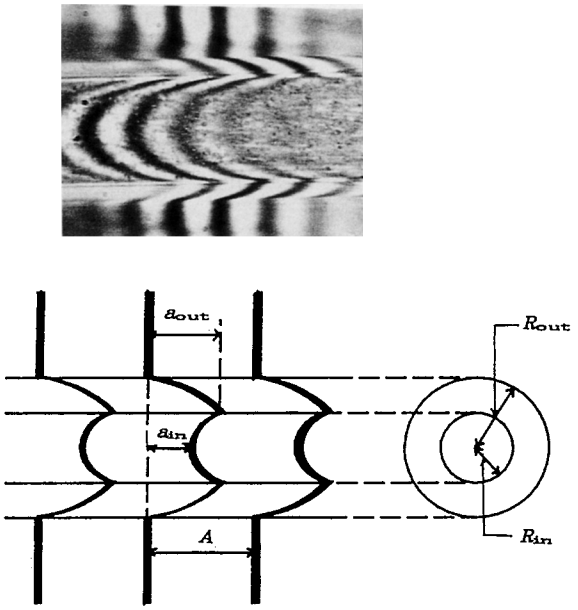

Figure 2 Typical optical micrograph and schematic illustration of interference fringe pattern observed under an interference microscope for a high-speed spun bicomponent fiber.

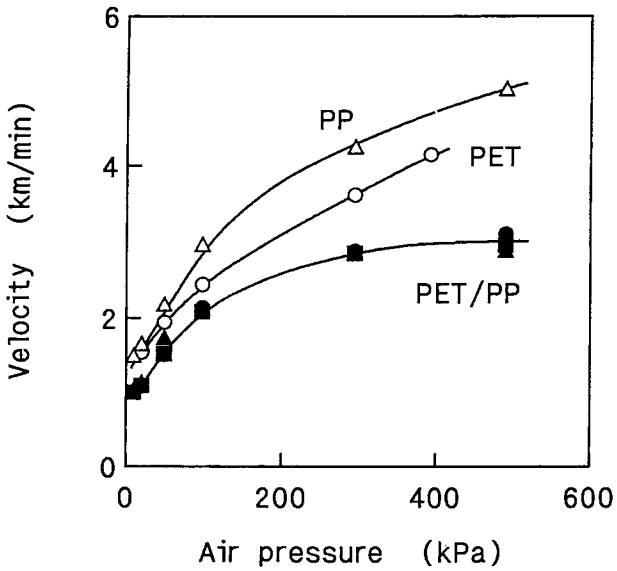

Figure 3 Relation between spinning velocity and air pressure applied to the air-ejector: PET/PP = (○) 10 : 0, (●) 7 : 3, (■) 5 : 5, (▲) 4 : 6, and (△) 0 : 10.

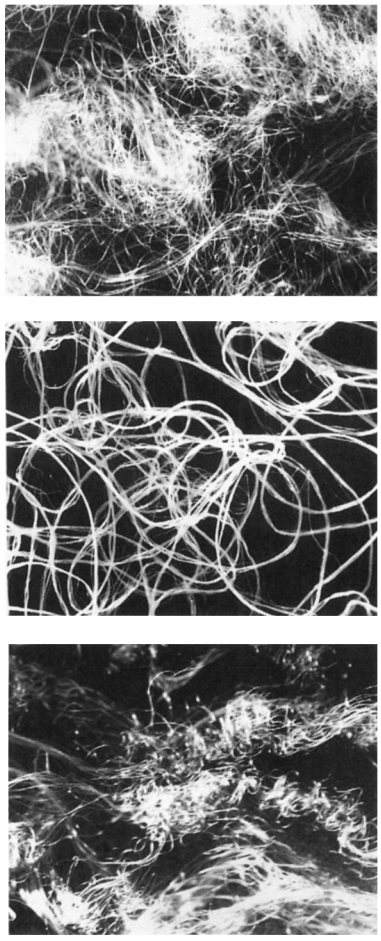

Figure 4 Photographs showing the appearance of as-spun single- and bicomponent filaments.

1.5 m below the spinneret, where the air-ejector was set, was expected to be close to the ambient temperature. This suggests that the sheath part of the bicomponent filament, PP, is still in a molten or rubbery state in the spinline even after cooling down to room temperature. This observation indicates that the structure formation of the PP component in the bicomponent spinning is significantly different from that of the single component PP.

Structural Characteristics of the As-spun Fibers

Figure 5(a) and (b) shows the birefringence of the PET and PP components, respectively, in the bicomponent fibers in comparison with the single-component fiber birefringence. Birefringence of the PET and PP single-component fibers increased with increasing spinning speed as reported previously.[17,18] The increase in the birefringence of the PET component in the PET/PP systems with the spinning speed was much steeper than that in the single-component spinning. It can also be seen that the birefringence of the PET component increased with decrease in the PET composition. On the other hand, the birefringence of the PP component is significantly lower than that of the corresponding single-component fiber. In other words, in the bicomponent spinning of PET and PP, the molecular orientation of the PET component is enhanced while the molecular orientation of the PP component remains very low in comparison with the corresponding single-component fibers.

According to the Lorentz–Lorenz equation given below, the Lorentz density, $(n^2 - 1)/(n^2 + 2)$, has a linear relation with the density, d:

$$\frac{n^2 - 1}{n^2 + 2}\frac{M}{d} = \frac{4}{3}\pi NP \tag{3}$$

where M is the molecular weight; N, Avogadro's number; and P, the molar polarizability. The mean refractive index n can be obtained from the measured refractive indices in the parallel and perpendicular directions, n_{para} and n_{perp}, using the following equation[19]:

$$n^2 = \frac{n_{para}^2 + 2n_{perp}^2}{3} \tag{4}$$

The estimated Lorentz density for PET single-component spinning and for the PET in PET/PP systems are given in Figure 6. The Lorentz density for PET single-component spinning started to increase at a take-up velocity of about 4 km/min, indicating the onset of orientation-induced crystallization. The Lorentz density of PET in the PET/PP systems

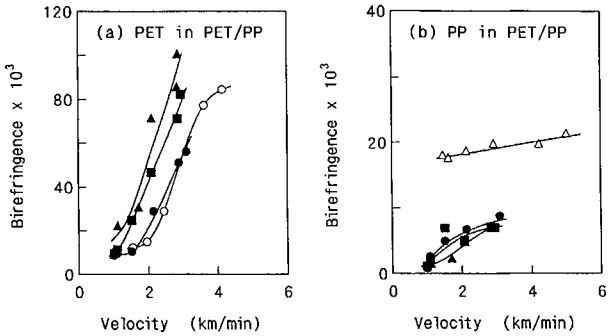

Figure 5 Birefringence of (a) PET and (b) PP components in single- and bicomponent fibers as a function of spinning velocity for various PET/PP mass flow rate combinations. PET/PP = (○) 10 : 0, (●) 7 : 3, (■) 5 : 5, (▲) 4 : 6, and (△) 0 : 10.

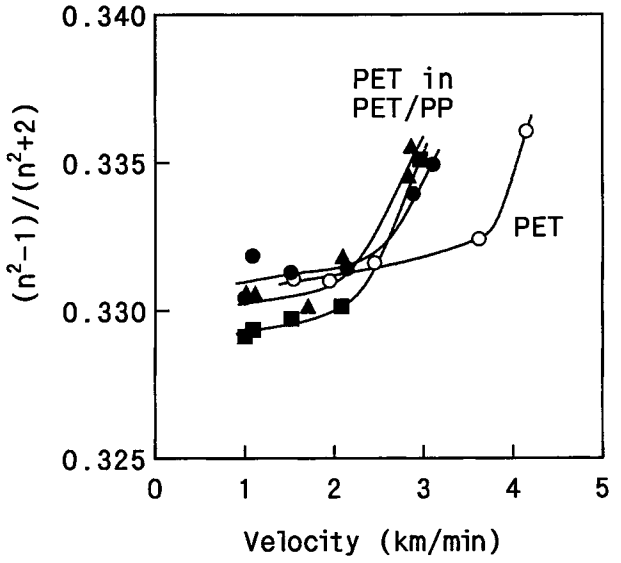

Figure 6 Variation of Lorentz density, $(n^2 - 1)/(n^2 + 2)$, with spinning velocity for PET component. PET/PP = (○) 10 : 0, (●) 7 : 3, (■) 5 : 5, and (▲) 4 : 6.

registered a steep increase at a lower take-up speed range in comparison with the single-component spinning. This observation suggests that the enhanced molecular orientation in the PET component during the bicomponent spinning also promotes the orientation-induced crystallization.

Evidence for the enhanced and suppressed structural development in the PET and PP components, respectively, also comes from the WAXD studies. An examination of the WAXD photographs shown in Figure 7 revealed that the orientation-induced crystallization of the PET component in PET/PP fiber has already started at around 3 km/min, which is lower in comparison with the single-component spinning. However, the PP component showed a pseudohexagonal structure even at a high-speed range where single-component fibers show a highly oriented monoclinic structure.

The above analyses clearly brings out the significant difference in the structure development during single-component and bicomponent fiber spinning. In the present bicomponent system of PET and PP, the structure development in the PET component was enhanced and significantly higher molecular orientation and orientation-induced crystallization were achieved at higher take-up speeds, whereas the PP component remained in a low orientation state and showed a pseudohexagonal structure. The sticking of PET/PP bicomponent filaments shown in Figure 4 was evidently brought about by the suppression of the crystallization of the sheath component, PP.

The considerable difference in the structural development during the bicomponent spinning may be attributable to the mutual interaction of the two polymers coextruded to form a single filament. To gain an understanding of the mechanism of structure development during the bicomponent spinning, a semi-quantitative numerical simulation was performed.

Semiquantitative Numerical Simulation

Newtonian Fluid Model

A steady-state model for single-component spinning, described in detail elsewhere,[13,18,20,21] was extended to the bicomponent spinning. It was assumed that there are no temperature and velocity distributions in the cross section of the bicomponent filament. The governing equations used for the simulation of the bicomponent spinning are given below:

Mass balance equation:

$$W = W_1 + W_2 = (\rho_1 A_1 + \rho_2 A_2)v \tag{5}$$

Momentum balance equation:

$$\frac{dF}{dx} = \frac{dF_1}{dx} + \frac{dF_2}{dx} = (W_1 + W_2)\left(\frac{v}{dx} - \frac{g}{v}\right) + \pi D\tau_f \tag{6}$$

where $D = 2[(A_1 + A_2)/\pi]^{1/2}$.

Energy balance equation:

$$\frac{dT}{dx} = -\frac{\pi Dh}{Cp_1 W_1 + Cp_2 W_2}(T - Ta) \tag{7}$$

Constitutive equation:

$$\frac{dv}{dx} = \frac{F_1 + F_2}{A_1\eta_1 + A_2\eta_2} \tag{8}$$

where F, v, D, and T denote the spinline tension, axial velocity, diameter, and temperature of the filament at a distance x from the spinneret. W is the mass flow rate and A is the cross-sectional area. ρ, η, and Cp are the density, elongational viscosity, and specific heat of the polymer. Subscripts 1 and 2 represent the two components in the bicomponent spinning. g is the acceleration due to gravity; τ_f, the shear stress on the surface of the filament related to the air friction; h, the heat transfer coefficient; and Ta, the ambient temperature.

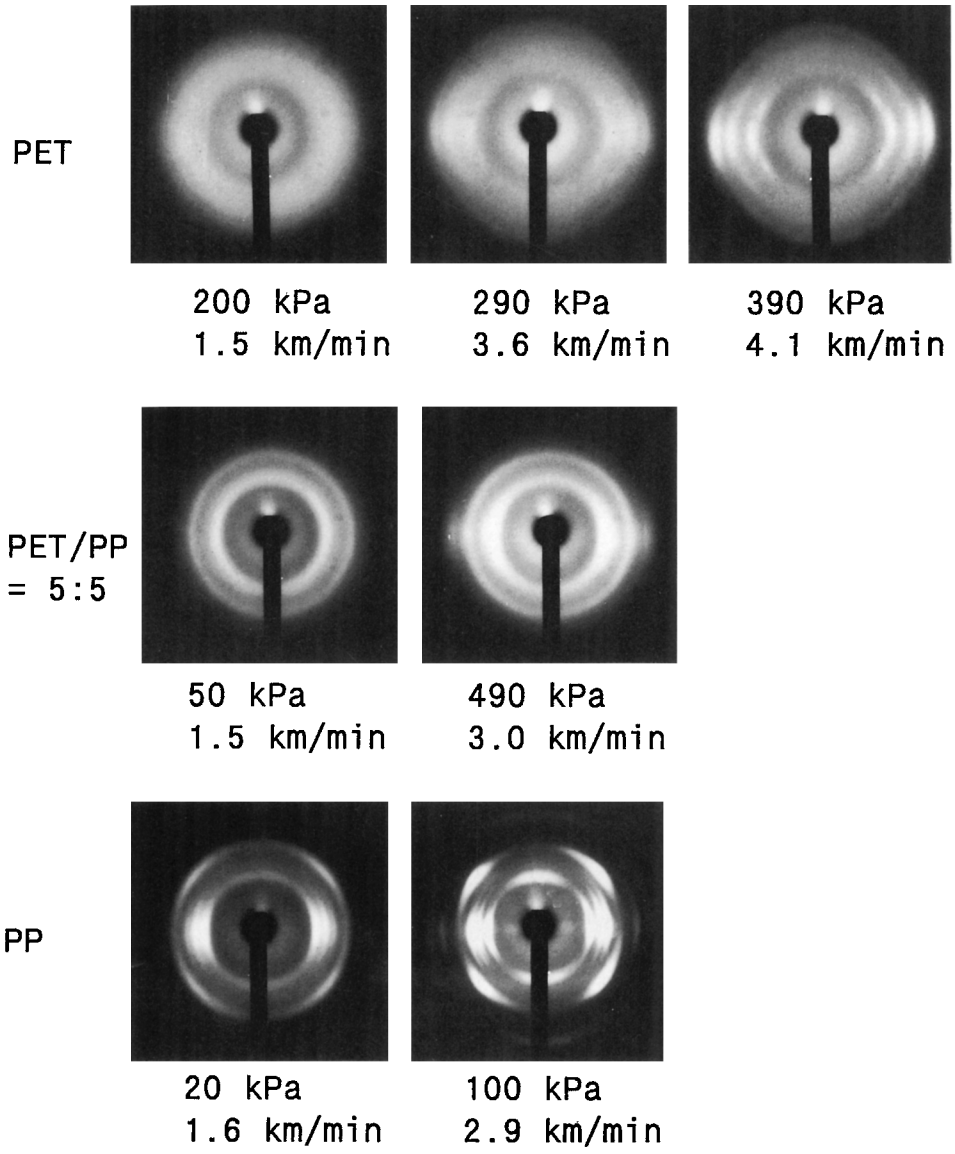

Figure 7 Comparison of the WAXD patterns of single- and bicomponent fibers.

Numerical simulations for the single- and bicomponent spinning were carried out by assuming that the PP and PET behave as a Newtonian fluid in the spinline with a temperature dependence of elongational viscosity shown in Figure 8.[18,22] These are the empirical relations based on the on-line measurements of diameter profile and tension in the melt spinning process. The data for PP and PET are from the materials with MFR of 30 and $[\eta]$ of 0.69 dL/g, respectively. Since these values are not far apart from those for the polymers used in the present work, the data in Figure 8 can be considered to represent the characteristics of the materials used.

In the present case, we used 70°C as the solidification temperature for both polymers, PET and PP. The other formulas and parameters used for the simulation are summarized in Table I.

The calculated diameter profiles for PP, PET, and PET/PP at a take-up speed of 1 km/min are given in Figure 9. The diameter profile of PET/PP was found to be lying between those of the PP and PET single-component spinning. The thinning behavior of a polymer in the spinline depends, besides many parameters, on the temperature dependence of elongational viscosity (activation energy) and the specific heat Cp of the polymer. In the case of single-component spinning, PET, which has a higher activation energy of elongational viscosity and a smaller Cp, solidifies at a position closer to the spinneret and shows a steeper thinning behavior as

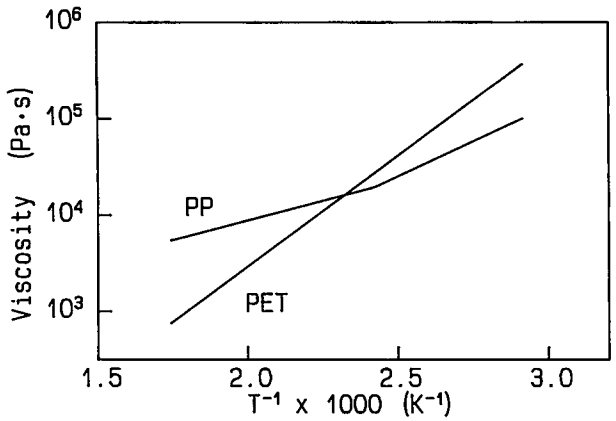

Figure 8 Temperature dependence of elongational viscosity for PET and PP used for simulation.

compared to the mild thinning behavior of PP which has a lower activation energy and a higher *Cp*. When these two polymers are coextruded to form a single filament of a sheath–core type, the thinning behavior was found to be between the two, apparently due to the additivity of the properties of both the components.

The calculated elongational spinline stress of PET and PP components in the PET/PP system at a take-up speed of 1 km/min are given in Figures 10(a) and (b) along with that of the corresponding single-component spinning. Near the spinneret, the spinline stress applied to the PET component in the PET/PP system was lower than that of the PET single-component spinning. The low spinline stress in this region is attributable to the restrained deformation of the spinline. The spinline stress, however, increased steeply along the spinline and eventually exceeded the stress in the single-component spinning. This result corresponds to the promoted spinline deformation observed in the diameter profile near the solidification point. Oppositely, near the spinneret, the spinline stress of the PP component in PET/PP system was higher than that of the single-component spinning. It subsequently exhibited a maximum and decreased slightly near the solidification point where single-component spinning showed a higher spinline stress.

Lipscomb[16] also made a similar observation: While analyzing the nonisothermal spinning of hollow fibers in the thin filament limit, he replaced the gas in the core with a temperature-dependent viscous liquid and found that the sheath stress profile showed a maximum and decreased in the draw zone contrary to the results found in single-component spinning and hollow fiber spinning with a core gas. He explained that such behavior is due to the ability

Table I Spinning conditions, Material Properties, and Aerodynamic Formulas and Parameters Used for the Simulation

Spinning conditions	
Mass out flow rate	$W = 1.0$ g/min
Spinneret diameter	$D_0 = 0.3$ mm
Spinning temperature	$T_0 = 290°C$
Ambient temperature	$T_a = 20°C$
Material parameters	
Density	
PET	$\rho = 1.356 - 5.0 \times 10^{-4}\, T$ (g/cm³)
PP	$\rho = 0.912 - 4.8 \times 10^{-4}\, T$ (g/cm³)
Specific heat	
PET	$Cp = 1.25 + 2.5 \times 10^{-3}\, T$ [J/(g K)]
PP	$Cp = 2.72$ [J/(g K)]
Formulas and parameters for heat transfer and air friction	
Heat-transfer coefficient	$h = ka\, Nu/D$
Nusselt number	$Nu = 0.42\, Re^{0.334}$
Air-friction stress	$\tau_f = (\frac{1}{2})\, \rho a\, v^2\, C_f$
Air-friction coefficient	$C_f = 0.37\, \mathrm{Re}^{-0.61}$
Reynolds number	$Re = D\, V/\nu_a$
Thermal conductivity of air	$k_a = 28$ mJ/(m s K)
Density of air	$\rho_a = 1.2$ kg/m³
Kinematic viscosity of air	$\nu_a = 16$ mm²/s

of the core to bear a greater fraction of the spinline tension if the core viscosity increases faster than does the clad as the temperature decreases.

Figure 11(a) and (b) shows the calculated solidification stress of PET and PP components in the PET/PP system, respectively, for various take-up

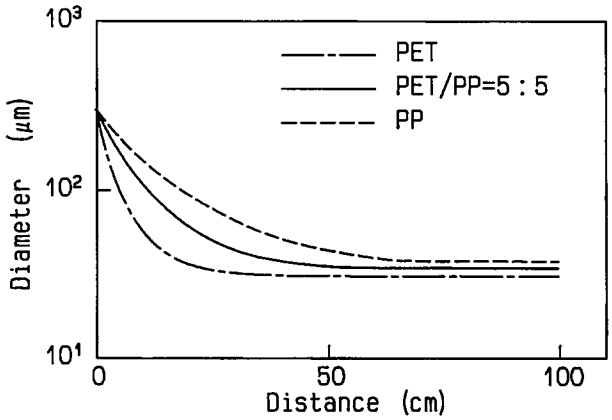

Figure 9 Predicted diameter profiles for the single-component spinning of PET and PP and bicomponent spinning of PET/PP = 5 : 5 at a take-up velocity of 1 km/min (Newtonian model).

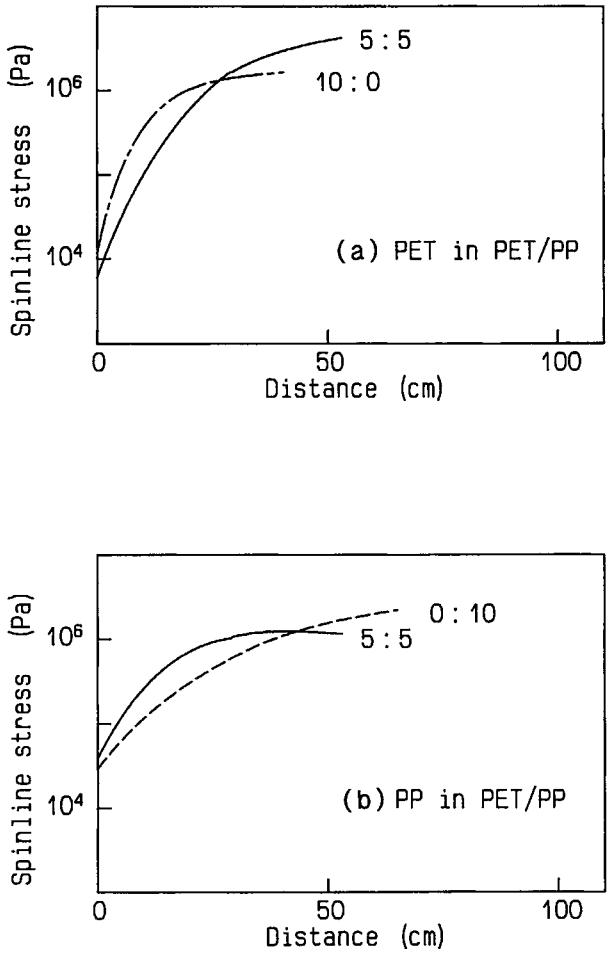

Figure 10 Predicted spinline stress profiles at a take-up velocity of 1 km/min for (a) single-component PET and PET in PET/PP = 5 : 5 and (b) single-component PP and PP in PET/PP = 5 : 5.

speeds and for various mass flow rate combinations. Solidification stress for the corresponding single-component spinning is also included for comparison. As observed earlier, there is a significant enhancement of solidification stress in the PET component for all the take-up velocities in comparison with single-component spinning. The solidification stress showed an increasing tendency as the composition of the PET component decreased. On the other hand, the solidification stress in the PP component was considerably lower than that of the single-component spinning. In both cases, the differences were much higher at higher take-up speeds. These results agreed in essence with the experimentally obtained molecular orientation of each component in bicomponent fibers shown in Figure 5. Therefore, it can be said that the simple Newtonian model provides a general idea about the mutual interaction of two components in spinline dynamics of the high-speed bicomponent fiber spinning.

As mentioned earlier, an identical solidification temperature of 70°C was assumed both for PET and PP components in these calculations. This temperature corresponds to the glass transition temperature of PET. Solidification of the spinning line of PP under usual spinning conditions was also reported to occur at around 70°C.[18] However, the solidification temperature of PP can change considerably if the melt spinning is performed under some specific spinning conditions as the solidification of PP occurs due to its crystallization. Thus, the assumption of the same solidification temperature for both polymers may not be adequate in some cases. Nevertheless, this assumption is unavoidable in the calculation using the Newtonian fluid model, be-

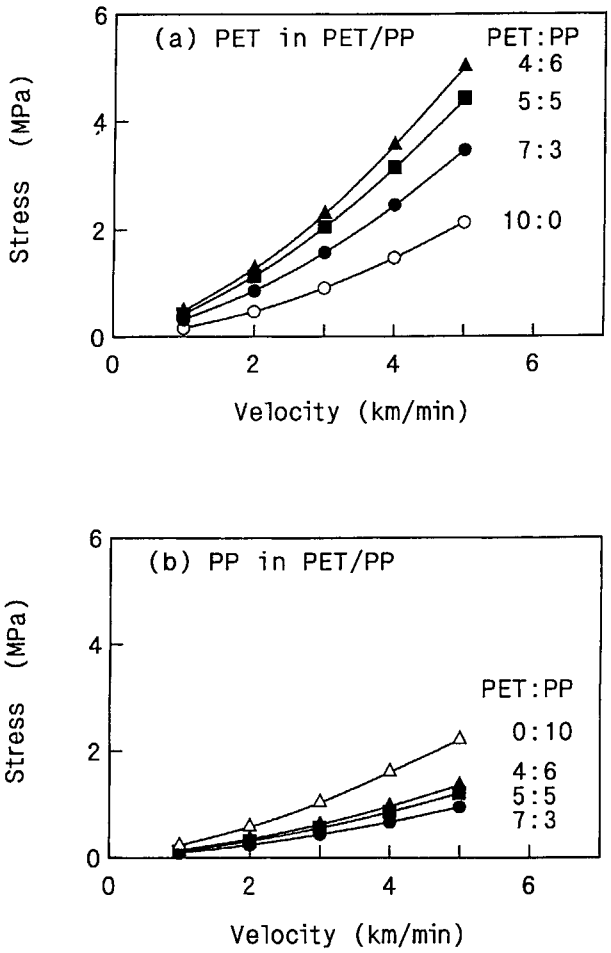

Figure 11 Calculated solidification stresses as a function of spinning velocity for various mass flow rate combinations (Newtonian model): (a) single-component PET and PET in PET/PP; (b) single-component PP and PP in PET/PP.

cause if one component solidifies at a certain temperature where the other component is still in a molten state, the elongational stress experienced by the latter vanishes instantly as further deformation of the spinline can not occur beyond that position. From a practical point of view, there is a possibility of stress relaxation occurring in the second component. To take into account this aspect in the simulation, a viscoelastic constitutive equation should be adopted.

Upper-convected Maxwell Model

The upper-convected Maxwell model incorporating the non-isothermal conditions was shown by Marrucci as follows[23]:

$$\sigma + \lambda\left[\frac{\partial \sigma}{\partial t} + \mathbf{v}\cdot\nabla\sigma - (\nabla\mathbf{v})\cdot\sigma - \sigma\cdot(\nabla\mathbf{v})T - \sigma\frac{\partial \ln T}{\partial t} - \sigma(\mathbf{v}\cdot\nabla \ln T)\right] = \mu[\nabla\mathbf{v} + (\nabla\mathbf{v})^T] \quad (9)$$

where σ is the extra stress; λ, the relaxation time; $\mathbf{v}$, the velocity; T, the temperature; μ, the viscosity; and t, the time. In a steady-state spinning condition, eq. (9) can be simplified to the following two-component equations[24]:

$$\tau + \lambda\left[v\frac{d\tau}{dx} - 2\tau\frac{dv}{dx} - v\tau\frac{d \ln T}{dx}\right] = 2\mu\frac{dv}{dx} \quad (10)$$

$$\omega + \lambda\left[v\frac{d\omega}{dx} + \omega\frac{dv}{dx} - v\omega\frac{d \ln T}{dx}\right] = -\mu\frac{dv}{dx} \quad (11)$$

where τ is the axial stress, ω is the stress normal to the spinning direction, and $\tau - \omega$ corresponds to the spinline stress, F/A.

In the case of bicomponent spinning, the following equation can be obtained from the eqs. (10) and (11) for both the components:

$$\left(\frac{A_1}{\lambda_1}\eta_1 + \frac{A_2}{\lambda_2}\eta_2 + 3A_1\tau_1 + 3A_2\tau_2 - 2F\right)\frac{dv}{dx} = \mathrm{v}\frac{\mathrm{dF}}{\mathrm{dx}} + \frac{\mathrm{F}_1}{\lambda_1} + \frac{F_2}{\lambda_2} - Fv\frac{1}{T}\frac{dT}{dx} \quad (12)$$

where $\eta = 3\mu$ is the elongational viscosity. For each component, the following equation can also be derived:

$$\frac{d\tau_j}{dx} = \left(\frac{2\tau_j}{v} + \frac{2\eta_j}{3\lambda_j v}\right)\frac{dv}{dx} - \frac{\tau_j}{\lambda_j v} + \frac{\tau_j}{T}\frac{dT}{dx} \quad (13)$$

where $j = 1$ and 2 designate each component.

Combining eqs. (12) and (13) with the momentum balance and energy balance equations, i.e., eqs. (6) and (7), numerical simulation of bicomponent spinning was carried out. In these equations, the mutual interaction between two components arising from a radial normal stress difference was neglected. Since the system response is relatively insensitive to the choice of the initial condition of stress as suggested by Denn et al.,[25] the boundary condition for ω at the spinneret was arbitrarily assumed to be zero. Because of the lack of detailed knowledge on the viscoelastic properties of the polymers used, the relation shown in Figure 8 was adopted for the temperature dependence of elongational viscosity, and a constant modulus value was used for each polymer assuming a single relaxation time of 2 ms at a temperature of 290°C.[26]

For the simulation, the solidification temperature of PET was kept at 70°C. Considering the pseudo-hexagonal structure of PP shown in Figure 7, the PP component was assumed not to solidify until it was cooled down to room temperature. The calculated velocity and temperature profiles are given in Figure 12. The velocity and temperature profiles of bicomponent spinning fell between those of the single-component spinning, a behavior similar to that of the diameter profile of the Newtonian fluid model (Fig. 9). The stress profiles of PET and PP components in the bicomponent fibers along with those of the single component are given in Figure 13(a) and (b). It is worth noting that there is a significant amount of stress relaxation of the PP component after the solidification of the PET component.

In single-component high-speed spinning, the PET fiber crystallizes above a certain take-up velocity, and solidification temperature, i.e., crystallization temperature, of the spinline increases

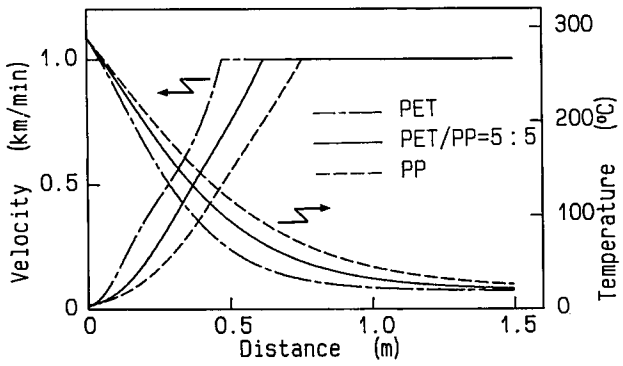

Figure 12 Predicted velocity and temperature profiles for single-component spinning of PET and PP and bicomponent spinning of PET/PP = 5 : 5 (Maxwell model).

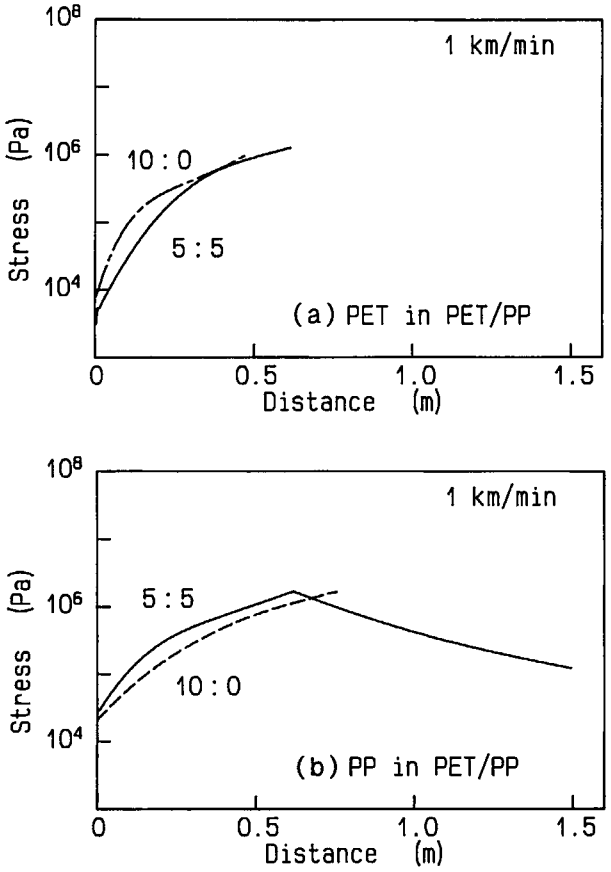

Figure 13 Predicted spinline stress profiles at a take-up velocity of 1 km/min for (a) single-component PET and PET in PET/PP = 5 : 5 and (b) single-component PP and PP in PET/PP = 5 : 5 (Maxwell model).

with increasing take-up velocity.[27] As shown in Figures 6 and 7, the PET component in the PET/PP bicomponent fiber also starts to crystallize above 3 km/min.

To incorporate the effect of crystallization, the simulation was performed simply assuming an abrupt solidification of the spinline at a predetermined crystallization temperature. Figure 14(a) and (b) shows the effect of the change of PET solidification temperature on the stress development for a take-up speed of 4 km/min. When the solidification temperature of PET was increased to 150°C, stress relaxation in PP was more prominent than that when the solidification temperature of PET was set at 70°C. Figure 15(a) and (b) summarizes the solidification stress of PET and PP components for various take-up speeds calculated with two PET solidification temperatures, 70 and 150°C. This result suggests that if the crystallization of PET occurs above a certain take-up speed molecular orientation of PP may saturate or take a maximum at that point.

In Figure 5(b), a tendency of saturation can be seen above 2–3 km/min. We have also reported, for the bicomponent spinning of the PET/polyethylene (PE) system, that the molecular orientation of PE had shown a distinct maximum at a take-up velocity where the crystallization of PET had started.[28]

Mechanism of Fiber Structure Development During the Bicomponent Spinning

The results obtained from the above-described numerical simulation clearly show that the mutual interaction of the two polymers coextruded to form a single filament is responsible for the significant differences in the fiber structure development during the bicomponent spinning as compared to that of the single-component spinning. The mutual interaction may be arising out of the differences in the

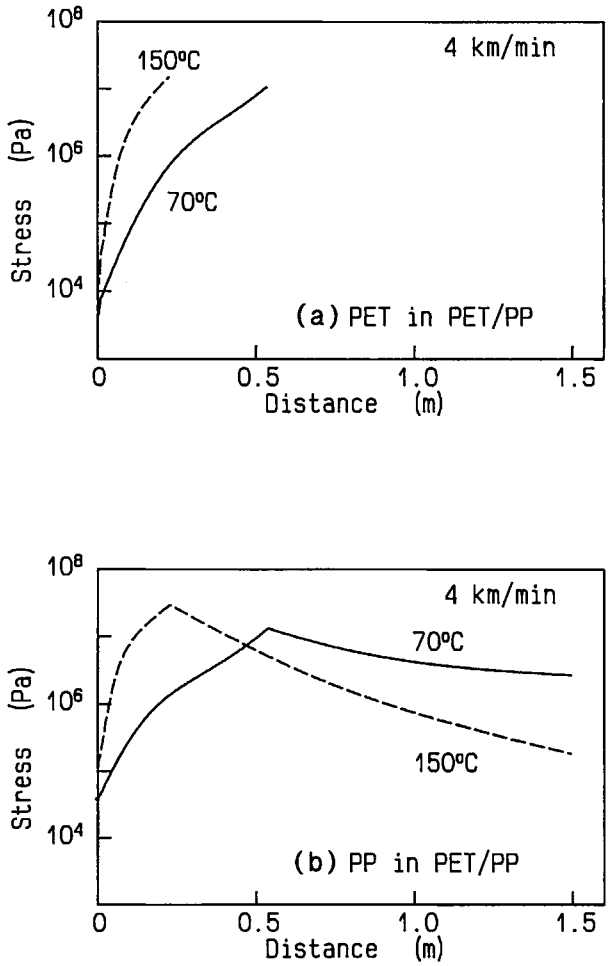

Figure 14 Predicted spinline stress profiles at a take-up velocity of 4 km/min for (a) PET and (b) PP in PET/PP = 5 : 5. Solidification temperature of PET component is 70 and 150°C (Maxwell model).

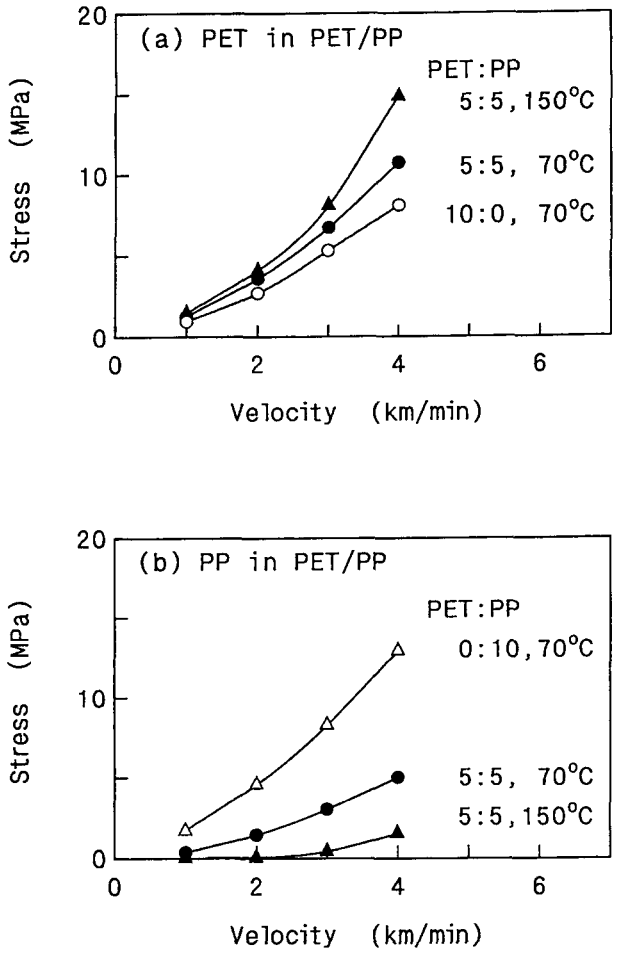

Figure 15 Calculated solidification stresses as a function of spinning velocity for PET solidification temperature of 70 and 150°C (Maxwell model): (a) single-component PET and PET in PET/PP = 5 : 5; (b) single-component PP and PP in PET/PP = 5 : 5.

inherent polymer characteristics of the component polymers. It may be noted that the temperature dependence of elongational viscosity (activation energy) of the two polymers used are different. In the present case, PET, which has a higher activation energy, may experience higher stress than in the case of single-component spinning in the downstream of the spinline. The higher levels of stress will also enhance the orientation and orientation-induced crystallization. On the other hand, the orientation development of the PP component which has lower activation energy may be suppressed. If the solidification of the PET component occurs while the PP component remains in a molten state, the PP component may undergo orientation relaxation. At the high-speed region, the solidification temperature of the PET component may increase because of the onset of orientation-induced crystallization. This leads to the further orientation relaxation of the PP component. The suppression of the orientation along with the high cooling rate at high spinning speeds prevents the occurrence of crystallization of the PP component even near room temperature and causes the sticking of running filaments. Since the glass transition temperature of PP is well below the room temperature, crystallization into a pseudohexagonal structure can be expected to occur even after the spinning process.

In closing, it should be noted that along with the above-mentioned two main factors for the mutual interaction in bicomponent spinning some additional factors should be considered if two components have a significantly different magnitude of elongational viscosity. In the high-speed melt spinning, the spinline tension increases with increasing distance from the spinneret because of the addition of inertia and air-friction forces. The effect of these forces on the spinline dynamics varies with the magnitude of elongational viscosity. Therefore, there can be some mutual interaction between two materials which have the same activation energy but significantly different viscosity values. This factor will be discussed in our forthcoming article.[29]

CONCLUSIONS

High-speed bicomponent spinning of PET (core) and PP (sheath) was carried out and the structure of the as-spun fibers was investigated. It was found that the PET component in the bicomponent fibers has an orientation and crystallinity higher than those of the PET single-component spun fibers, whereas the PP component remained in a low orientation state and had a pseudo-hexagonal structure even up to high take-up speeds. A semi-quantitative numerical simulation was performed and the results obtained using the Newtonian fluid model showed that the solidification stress of the PET component increases while that of the PP component decreases. This was attributed to the difference in the activation energy of elongational viscosity between two polymers. To take into account the stress relaxation occurring in the PP component after the solidification of PET, an upper-convected Maxwell model was taken as the constitutive equation. The results showed that considerable stress relaxation of the PP component occurs if the PET component solidifies while the PP component is in a molten state. This relaxation effect may be enhanced after the onset of the orientation-induced crystallization of

PET. Based on the structural characterization data and the simulation results, a mechanism for structure development was proposed for high-speed bicomponent spinning.

REFERENCES

1. T. Nakajima, Ed., *Advanced Fiber Spinning Technology,* Woodhead, Cambridge, 1994.
2. A. Ziabicki, *Fundamentals of Fiber Formation,* Wiley, New York, 1976.
3. A. Ziabicki and H. Kawai, Eds., *High-speed Fiber Spinning,* Wiley, New York, 1985.
4. C. D. Han, *J. Appl. Polym. Sci.,* **17,** 1289 (1973).
5. A. E. Everage, Jr., *Trans. Soc. Rheol.,* **17**(4), 629 (1973).
6. J. H. Southern and R. L. Ballman, *Appl. Polym. Sci.,* **20,** 175 (1973).
7. D. L. MacLean, *Trans. Soc. Rheol.,* **17**(3), 385 (1973).
8. J. H. Southern and R. L. Ballman, *J. Polym. Sci. Polym. Phys. Ed.,* **13,** 863 (1975).
9. M. C. Williams, *AIChE. J.,* **21,** 1204 (1975).
10. S. Tomioka and M. Kojima, *Sen'i Gakkaishi,* **36,** T-201 (1980).
11. S. Tomioka and M. Kojima, *Sen'i Gakkaishi,* **35,** T-542 (1979).
12. W. S. Lee and C. W. Park, *Int. Polym. Process.,* **9,** 3359 (1994).
13. J. Shimizu, N. Okui, and T. Kikutani, *High-speed Fiber Spinning,* A. Ziabicki and H. Kawai, Eds., Wiley, New York, 1985, p. 173.
14. T. Kikutani, *Sen'i Gakkaishi,* **50,** P-529 (1994).
15. C. W. Park, *AIChE. J.,* **36,** 197 (1990).
16. G. G. Lipscomb, *Polym. Adv. Tech.,* **5,** 745 (1994).
17. J. Shimizu, N. Okui, and T. Kikutani, *Sen'i Gakkaishi,* **37,** T-135 (1981).
18. J. Cao, T. Kikutani, A. Takaku, and J. Shimizu, *J. Appl. Polym. Sci.,* **37,** 2683 (1989).
19. M. F. Vuks, *Opt. Spectrosc.,* **20,** 361 (1966).
20. S. Kase and T. Matsuo, *J. Polym. Sci. A3,* 2541 (1965).
21. S. Kase and T. Matsuo, *J. Appl. Polym. Sci.,* **11,** 251 (1967).
22. I. Hamana, *Formation of Fibers and Development of Their Structure,* The Soc. Fiber Sci. Tech., Japan, Kagakudojin, Kyoto, 1969, p. 123.
23. G. Marrucci, *Trans. Soc. Rheol.,* **16**(2), 321 (1972).
24. R. J. Fisher and M. M. Denn, *AIChE J.,* **23,** 23 (1977).
25. M. M. Denn, C. J. S. Petrie, and P. Avenas, *AIChE J.,* **21,** 791 (1975).
26. D. R. Gregory, *Trans. Soc. Rheol.,* **17**(1), 191 (1973).
27. K. Fujimoto, K. Iohara, S. Owaki, and Y. Murase, *Sen'i Gakkaishi,* **44,** 53 (1988).
28. T. Kikutani, S. Arikawa, A. Takaku, and N. Okui, *Sen'i Gakkaishi,* **51,** 408 (1995).
29. J. Radhakrishnan, T. Kikutani, and N. Okui, to appear.

Received March 14, 1996
Accepted July 5, 1996